Monolithic transparent 3D dielectrophoretic micro-actuator fabricated by femtosecond laser

Tao Yang and Yves Bellouard

Galatea Lab, STI/IMT, Ecole Polytechnique Fédérale de Lausanne (EPFL), 2002 Neuchatel, Switzerland

E-mail: tao.yang@epfl.ch

CrossMark

Abstract

We demonstrate a three-dimensional (3D) monolithic micro-actuator fabricated by non-ablative femtosecond laser micromachining and subsequent chemical etching. The actuating principle is based on dielectrophoresis. An analytical modeling of this actuation scheme is conducted, which is capable of performance prediction, parameter optimization and instability analysis. Static and dynamic characterizations are experimentally verified. An actuation range of 30 μm is well attainable; resonances are captured with an evaluated quality factor of 40 (measured in air) and a bandwidth of 5 Hz for the primary vertical resonance of 200 Hz. A settling time of 200 ms in transient response indicates the damping properties of such actuation scheme. This actuation principle suppresses the need for electrodes on the mobile, non-conductive component and is particularly interesting for moving transparent elements. Thanks to the flexibility of the manufacturing process, it can be coupled to other functionalities within monolithic transparent micro-electro-mechanical systems (MEMS) for applications like tunable optical couplers.

Keywords: monolithic 3D actuators, femtosecond laser micromachining, dielectrophoresis actuation, optomechanics, transparent actuators

(Some figures may appear in colour only in the online journal)

1. Introduction

An actuator is a type of device that is operated by a source of energy and converts that energy into motion and/ or force in a controllable and preferably, in a reversible way. At the micro-scale, actuators have been extensively investigated and are part of a sub-class of micro-electro-mechanical systems (MEMS). Micro-actuators are ubiquitous and find applications in various fields as diverse as micro/ nano manipulation, precise and fast speed positioning as well as dynamic motion control. Reviews of micro-actuation principles can be found for instance in [1, 2].

However and essentially due to the lack of suitable manufacturing processes, micro-actuators remain essentially planar devices; furthermore, they often require cumbersome fabrication process involving multiple steps that reduce their integration potential into more compact and more cost-effective ensemble.

In optomechanics, the number of actuation principles suitable for optical devices in the visible ranges remains limited. Nonetheless, they are of high interest for various optical applications like optical microscopy, tunable optical devices for waveguide coupling, near-field probes as well as adaptive optics for high-power lasers. As an attempt to fill some of these gaps, actuation principles for instance based on electrowetting [3], magnetofluidic actuation [4] as well as transparent electrostatic actuation [5] have been proposed. However, a simple, generic actuation principle, with yet three-dimensional (3D) capabilities is still missing.

To advance the field of actuators suitable for optics operating in the visible ranges, here, we investigate a monolithic transparent 3D actuator fabricated by non-ablative
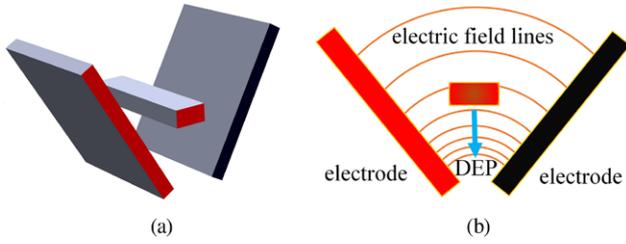
Figure 1. (a) 3D rendering of the V-shape groove and the cantilever. (b) Dielectrophoresis actuation of the cantilever.

femtosecond laser and chemical etching that uses dielectrophoresis force as actuation principle.

Femtosecond laser micro-machining and subsequent chemical etching, using potassium hydroxide (KOH) or hydrogen fluoride (HF), has emerged as a promising method to fabricate monolithic and 3D devices that combine multiple functions, like optical, fluidic, mechanical and optical functions. The processing consists of using laser emitting ultrashort pulses to locally tailor material properties so that laser exposure areas can be either etched away or modified with sub-wavelength spatial resolutions to acquire specific physical properties that were no present at first. Thanks to the nonlinear absorption phenomena taking place during laser exposure, a unique characteristic of this process is the possibility to modify material properties in the 3D and in particular below the material surface.

Dielectrophoresis or 'DEP', first termed by Pohl [6] in the early 1950s, is defined as the electrostatic action on dielectrics, due to an induced dipole moment under a non-uniform electric field. As an actuation method, the most common application is to manipulate and to sort micro-particles [7]. Recently, this realm has been extended to optomechanics enabling nano-mechanical functionality inside optical fiber [8] as well as nano-beam actuation [9].

A roadblock to DEP implementation is the need for nontrivial shapes, eventually 3D ones, that makes it difficult to manufacture with conventional techniques. Benefitting from 3D manufacturing capability of femtosecond laser, here we demonstrate a monolithic DEP actuator that we characterize analytically and experimentally.

2. Working principle, fabrication and modeling

2.1. Working principle

As a proof-of-concept, we investigate a cantilever moving in a non-uniform electrostatic field created by a V-shape arrangement of electrodes. This concept is inspired from R. Jebens and co-workers [10] who suggested this idea for positioning an optical fiber. Here, we generalize the concept proposed conceptually by Jebens and further demonstrate it on a monolithic design, theoretically and experimentally.

The working principle is briefly outlined in figure 1. When an external driving voltage is applied on both sides of the V-shape groove, a non-uniform electric field rises as indicated by the field lines in figure 1(b). The presence of the electrostatic field causes the appearance of an effective dipole moment in the cantilever. Since the electrostatic field is non-uniform, a

net force appears distributed along the cantilever causing the slim structure to bend.

2.2. Fabrication

The actuator includes a cantilever with a high aspect ratio of 1 : 300 symmetrically located in a V-shape groove fabricated out of a single piece of fused silica by femtosecond laser irradiation with subsequent HF etching illustrated in figure 2.

An overview of the fabrication processing is as followed. Laser exposure is provided by an ytterbium-fiber amplifier laser with pulse duration of 270 fs. The laser emits pulses of 230 nJ at a frequency of 800 kHz, corresponding to an average power of 184 mW. The laser beam is focused down to a beam waist about 1.5 μm using an objective with an effective numerical aperture of 0.4. The substrate is a 500 μm-thick fused silica (a-SiO$_2$). The specimen is loaded onto a dual axes motorized stage which enables plane motion, whereas the laser focal spot is translated by a Z-axis stage. Those three axes can achieve synchronized motion, thus achieving 3D-scanning of the laser focal point. Following the laser modification step, the specimen is immersed into a 2.5% concentration HF bath for pattern etching while keeping low tapered profile.

After etching, a cantilever of a length of 13 mm with a typical cross section of 90 μm × 30 μm is well attainable.

Both sides of the V-shape groove are coated with conductive layer, e.g. gold or indium tin oxide (ITO) for high transparency purpose, serving as electrodes. Before depositing the conductive layers, the machined pattern is partly covered by a masking tape. The mask is carefully designed to prevent bridging both sides of the V-shape groove and to insulate electrically the cantilever from either side of the groove.

2.3. Analytical model: force induced by the non-homogeneous electrostatic field

Effective dipole moment theory is adopted to determine the DEP force [11]. Its general governing expression on dielectrics in a non-uniform electric field is:

$$\vec{F} = C_\mathrm{V} \varepsilon_\mathrm{m} \mathrm{Re}(K) \vec{\nabla} \vec{E}^2 \qquad (1)$$

where C_V denotes the volume of object to be manipulated; ε_m the permittivity of medium; $\mathrm{Re}(K)$ the real part of the Clausius–Mossotti factor K and E the applied electric field. For non-spherical object, the resultant average dipole orientation needs to be considered by introducing a form factor B in the classical expression of the Clausius-Mossotti factor [12].

$$K = \frac{\varepsilon_\mathrm{p}^* - \varepsilon_\mathrm{m}^*}{2\varepsilon_\mathrm{m}^* + B(\varepsilon_\mathrm{p}^* - \varepsilon_\mathrm{m}^*)} \qquad (2)$$

where complex permittivity $\varepsilon^* = \varepsilon - j\,\sigma/\omega$. ε and σ denote permittivity and conductivity, respectively. ω is the angular frequency of electric field. Subscripts m and p denote air medium and fused silica, respectively.

For an elongated cantilever with its long axis normal to the plane defined by the electric field and the field gradient direction, the factor B is expressed as:
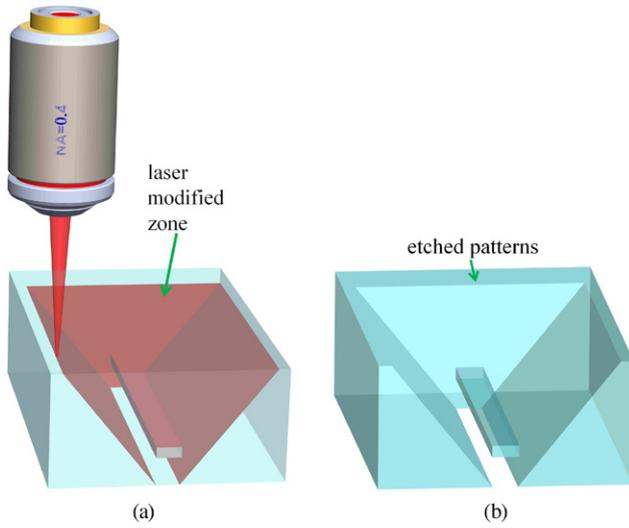
Figure 2. Illustration of the two steps of femtosecond laser processing combined with chemical etching. (a) First, the material is modified by a tightly forced femtosecond laser emitting low energy pulse, no ablation takes place. (b) The second step is to immerse the substrate into preferential chemical etching and to reveal the patterns.

$$B = lwb \int_0^\infty \frac{\mathrm{d}s}{(s + w^2)\sqrt{(s + l^2)(s + w^2)(s + b^2)}} \quad (3)$$

where l denotes the length which is normal to both electric field and field gradient; w is the width of the cantilever aligning with the electric field; b is the thickness parallel to the field gradient.

Generally, there is no explicit analytical solution for the gradient of an electric field, but in the particular case of V-shape boundary conditions in figure 3(b), it is given by [13]:

$$\vec{\nabla} \vec{E}^2 = \frac{2V^2}{r^3\theta^2} \vec{e_r} \quad (4)$$

where r is the distance between the cantilever center and the reference point defined in polar coordinate system with the reference point coincides with the virtual tip of the groove, θ is the opening angle of the V groove and V denotes the applied voltage. $\vec{e_r}$ is a unit vector.

Three parameters as in figure 4(a) are defined from the manufacturing point-of-view: the height h of the cantilever away from the bottom of the V groove, the smallest gap g between the two sides of the groove and the opening angle θ of the V-shape groove. Their relation is defined in equation (5) based on the assumption that the two electrodes are considered to be infinite planes. Considering the aspect ratio of the electrodes (15 mm × 0.7 mm), we can assume that this assumption is valid as a first order estimation and that fringe effects can be neglected.

As the chemical etching step can cause some deviations in the dimensions, parameters, measured after the fabrication process, are served as inputs for quantifying the force output.

$$F \propto \left(h + \frac{g}{2\tan(\theta/2)} \right)^{-3} \theta^{-2} \quad (5)$$

From the modeling, it is shown that the vertical distance h is of critical importance for achieving maximum magnitude of
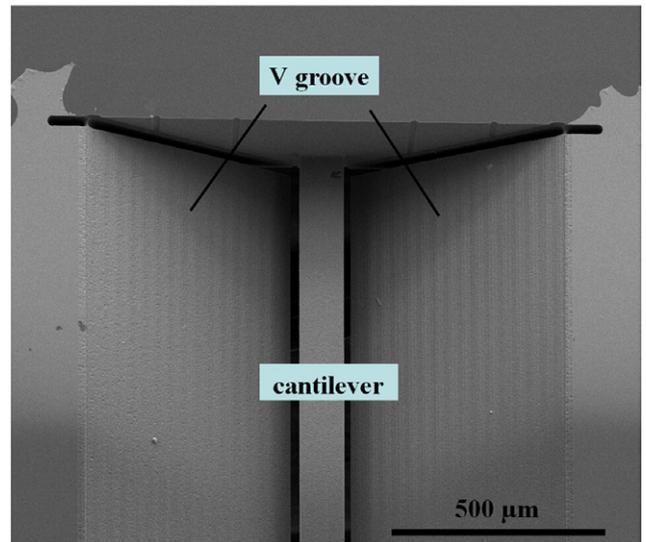
(a)
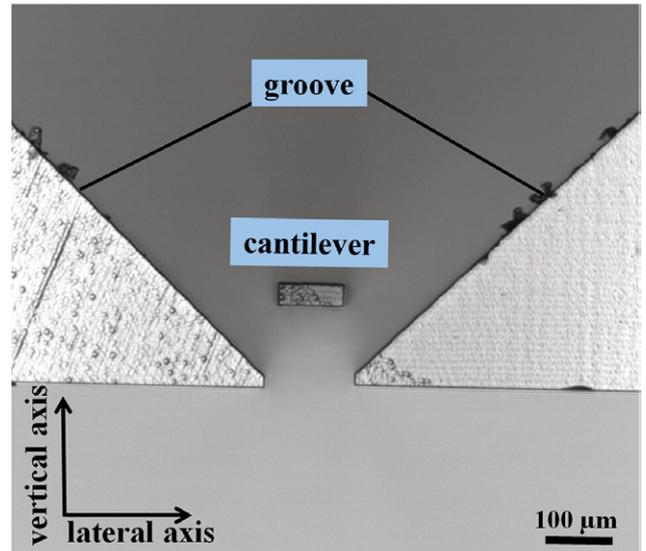
(b)

Figure 3. (a) Scanning electron microscopy image (SEM) of the V-shape groove surfaces and the cantilever top surface. (b) Microscopy image of the cantilever tip.

force. It is preferred to be as small as possible before meeting the limitations set by the traveling range and the width of the cantilever. The DEP force dependency on parameter θ is highly nonlinear. As shown in figure 4(b), as the gap g is much smaller than h, the DEP force gains sensitivity to the change of the angle and the optimal angle defining maximum DEP force lies in very narrow range; when the gap g grows bigger than h, the DEP force can be slightly increased by enlarging the angle.

2.4. Analytical model: mechanical stability of the cantilever-V-shape groove system

Pulling-in instability is a widely known limitation of electrostatic micro/ nano actuators due to an inherent nonlinearity of electromechanical coupling. Instability limits the traveling

(a)

(b)
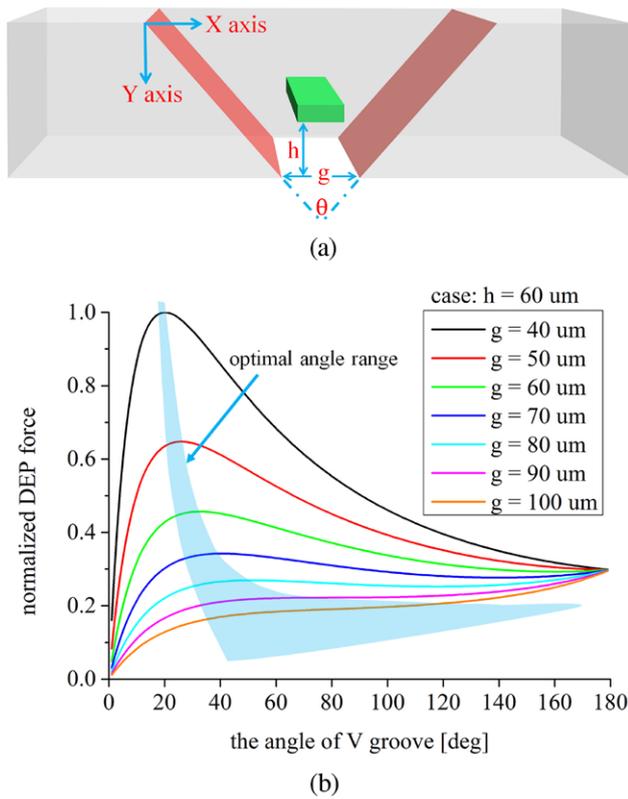
Figure 4. (a) Diagram of design parameters of the V-shape groove. (b) Optimal angle range with respect to variable gap g for a fixed h. We define the optimal angle as the one resulting in an enhanced magnitude of DEP force.

range and can cause the collapse of the devices. The DEP force is position dependent and varies as the cube of the reciprocal of the position of the cantilever defined in equation (4), while the spring restoring force increases linearly to the deflection. Like for classical electrostatic actuators, DEP actuators can also become unstable. Keeping the DEP actuator in a stable regime is an essential condition for operating the device.

The linear stiffness along the motion axis and expressed at the tip of the cantilever for uniform transverse loading is given by:

$$K_{\text{stiff}} = \frac{8EI}{l^3} \qquad (6)$$

where E is the Young's modulus of fused silica, I is the area moment of inertia. From equations (1) and (4), the DEP force can be expressed as:

$$\vec{F} = C_V \varepsilon_{\text{m}} \text{Re}(K) \frac{2V^2}{(r_0 - r_x)^3 \theta^2} \vec{e_y} \qquad (7)$$

where r_0 and r_x are the initial position and the deflection of the cantilever, respectively, the axes are as shown in figure 4(a). In mechanical equilibrium, the net force applied on the cantilever is zero, thus:

$$\left(\sum \vec{F} \right) \cdot \vec{e_y} = C_V \varepsilon_{\text{m}} \text{Re}(K) \frac{2V^2}{(r_0 - r_x)^3 \theta^2} - \frac{8EI}{l^3} r_x = 0 \qquad (8)$$
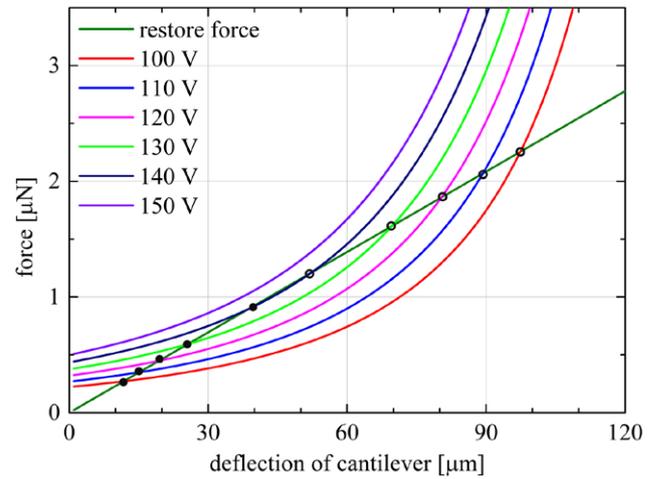
Figure 5. Plot of the DEP force and the mechanical restoring force. The intersections between them are the mechanical equilibrium positions. Bottom left intersections with black dots are mechanically stable equilibrium points whereas the top right points with hollow circles are instable and physically inexistent.

The instability position can be found by taking the derivative of the total net force with respect to the deflection of the cantilever: $\partial \Sigma \overrightarrow{F} / \partial r_x = 0$. Combining with equation (8), we can solve analytically the instability parameters: the critical driving voltage V_{pi} before pulling in and the instability position r_{pi} (here, the maximum deflection) expressed in equations (9) and (10).

$$r_{\text{pi}} = \frac{r_0}{4} \qquad (9)$$

$$V_{\text{pi}}^2 = \frac{27 r_0^4 \theta^2 K_{\text{stiff}}}{512 C_V \varepsilon_{\text{m}} \text{Re}(K)} \qquad (10)$$

Exploiting the analytical model we developed, the instability of V-shape DEP actuator is graphically presented. The mathematically positive solutions of the fourth order polynomial in equation (8) are shown graphically in figure 5.

Out of the two mathematical solutions shown with a black dot and a hollow circle, only the smaller one shown with a black dot is physically existent (indicated by equation (9)). When the driving voltage exceeds the critical value 142 V predicted by the modeling, stable positions will no longer exist and the cantilever can collapse to the V-shape boundaries or be dragged out of the V groove causing failures.

For the voltage-driven scheme of V-shape DEP actuators, the stable motion of the cantilever no longer exists beyond one fourth of r_0. The initial position r_0 needs to be increased in order to extend the traveling range, and as a consequence, higher driving voltage is required.

Compared with classical electrostatic actuators [14], which have a general form of the driving force $F_{\text{elec}} = \varepsilon_0 A V^2 / (2r^2)$ and a pulling in position at one third of the comb gap, we believe the dependency of the electrostatically driving force on the position limits the traveling range.

When the scale of the V-shape groove and the cantilever is changed isomorphically in the 3D, the relative influence of the DEP force and the mechanical force will be altered. The

gradient factor $\vec{\nabla}\,\vec{E}^2$ has a scaling factor of l^{-3} in terms of dimension l, by noticing that it has a unit of V^2/m^3 [15]. Thus, the overall DEP force scales as l^0, while maintaining the relative position of the cantilever with respect to the groove. On the other hand, the mechanical stiffness scales as l^1. Scaling advantages of the DEP force over the mechanical restore force exhibits as the actuator shrinks to smaller size. A much lower voltage will be needed comparatively for achieving the same ratio of displacement versus size of the V-shape groove. The actuator becomes also more sensitive to voltage variations.

3. Experiments and characterization

Performance metrics of the DEP actuator are examined by measuring the deflection of the cantilever tip. The static and dynamic characteristics, including static force output, static deflection, dynamic resonance and step response are reported. Different prototypes are manufactured, so that the performance falls within the average of different cases outlined in the previous paragraph.

3.1. Experimental methods

A camera system is designed to measure the static deflection of the cantilever tip. A direct voltage (dc) power supply (SRS, Inc. PS300) is used to provide a dc source up to 200 V; a calibrated camera system (Thorlabs DCC1645C) with white light source is adopted for imaging and measuring the static motion of the cantilever tip.

Since this camera system is insufficient for high frequency measurement, another optical setup based on position sensing detector (PSD) (First Sensor DL16-7-PCBA3) is used to characterize the dynamics of the actuator, illustrated in figure 6. Arbitrary wave output is generated by a function waveform generator (Agilent 33120A) and amplified by a constant gain high voltage amplifier (Falco Systems WMA-01) up to 120 V. A digital oscilloscope (Rigol DS1204B) is connected to the PSD for monitoring and recording the dynamic response of the actuator. To create a visible spot on the PSD, a Helium-Neon (HeNe) laser is transmitted through an optical fiber which itself is constrained and guided by a trench whose width is about the diameter of a single mode fiber. Since the trench is monolithically fabricated with the actuator, which enables accurate alignment between the fiber and the cantilever, an effective butt coupling between them initiates the transmission of the laser beam through the cantilever. The cantilever acts as a multimode waveguide and the transmitted light is projected onto the PSD sensing area by alignment using micro-stages, shown in figure 7. All experiments are performed under atmospheric pressure at room temperature.

3.2. Static response

The accuracy of the analytical model is tested by measuring the static deflection when an equilibrium position is reached. Figure 8 shows the measured and modeled deflections of the cantilever for various voltages. After applying a dc driving
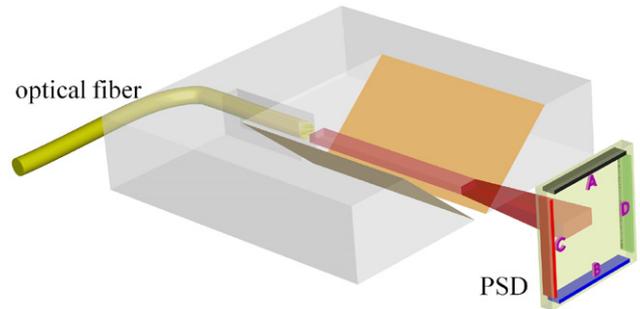
Figure 6. PSD and an optical coupling setup for measurement of DEP dynamics.
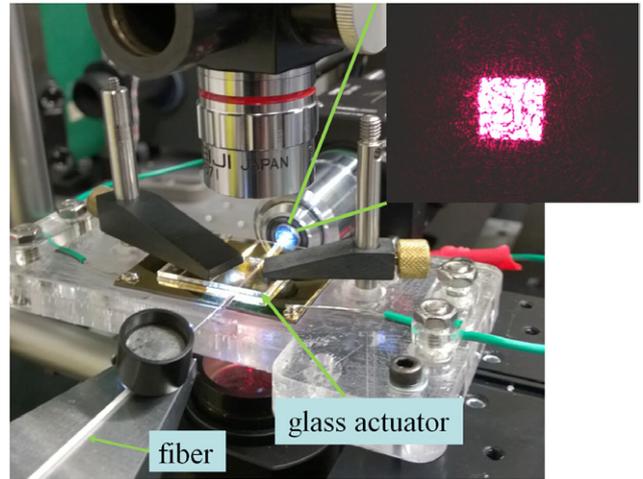
Figure 7. The cantilever motion is monitored by a PSD. This setup can also serve as a demonstrator for an optical coupler to fibers and an optical switch when electrically actuated. The top right image is the laser intensity distribution transmitted through a square cross section cantilever.
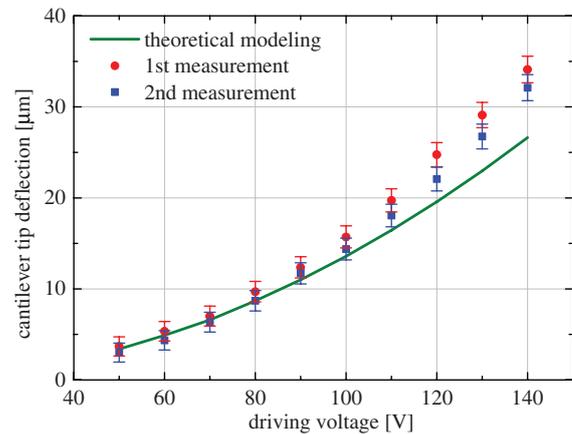
Figure 8. Experimental results and theoretical analysis of the cantilever deflection under dc.

voltage, the cantilever shows stable deflection towards high electric field. The deflection direction is independent of the sign of the voltage. This is a logical result from equations (1) and (4): changing the sign will reverse the direction of the electric field but not the gradient of the field. The cantilever also exhibits nonlinear deflection, which results from the fact that the deflection is proportional to the square of the electric

field. Experimental results and modeling show a good agreement. The variations between them can be caused by the first order approximation of the electric field magnitude and facts like the relatively low accuracy of the cantilever thickness. The calculated DEP force is in the order of a few μN mm^{-3} on the cantilever.

The two measurements in figure 8 were conducted at different times. Since the relative permittivity of air medium is strongly dependent on the environmental humidity as are the resistivity and the relaxation of air [16], this effect influences the overall dipolar polarization process and induces variations in measurement.

Collapse or 'dragged instability' takes place when the driving voltage surpasses the critical value 150 V in experiments. This critical voltage varies from case to case, highly depending on the design parameters.

3.3. Dynamic response

The DEP force is proportional to the square of the applied voltage as shown in equations (1) and (4). Supposing both dc and ac voltage are supplied:

$$V = V_{ac} + V_{dc}$$

$$V^2 = V_{dc}^2 + \frac{V_{ac}^2}{2} + 2V_{dc}V_{ac}\sin(\omega t) - \frac{V_{ac}^2\cos(2\omega t)}{2} \quad (11)$$

Generally, the resulting force applied on the cantilever contains terms in both $\cos(\omega t)$ and $\sin(\omega t)$, and it leads to the vibration of the cantilever between the initial position and the maximum amplitude position near the bottom of the V-shape groove. When the ac component dominates, the cantilever can be driven at twice the frequency of the applied ac voltage [17]. A sinusoidal driven voltage at 10 Hz is used to excite the actuator, the response of the cantilever tip vibration at 20 Hz is shown in figure 9.

Resonance frequencies offer an insight into the mass, damping and stiffness properties. The vibration modes of the DEP actuator are tested by frequency sweeping method at moderate magnitude of the driving voltage. dc voltage is supplied to set bias and ac voltage superimposed onto dc is used to excite the resonances. To predict the appearance of resonances, classical Euler-Bernoulli model is adopted [18].

$$EI\frac{\partial^4 y(x,t)}{\partial x^4} + \rho A\frac{\partial^2 y(x,t)}{\partial t^2} = f(x,t) \quad (12)$$

where $y(x,t)$ is the deflection from equilibrium axis in Cartesian coordinate, ρ is the density of fused silica, A denotes the area of cross section and $f(x,t)$ denotes the applied transverse force on per unit length of the cantilever. The natural resonance is expected to be at $\omega_0 = (1.875/l)^2\sqrt{EI/(\rho A)}$ with a second harmonic mode at about 6.2 ω_0. Due to manufacturing and design variations, the cantilever is not exactly located symmetrically inside the V-shape groove. As a consequence, a lateral force, tangent to the electric field lines can be present. First two resonances along both vertical and lateral directions are measured and shown in figure 10. The direction is the same as defined in figure 3(b).
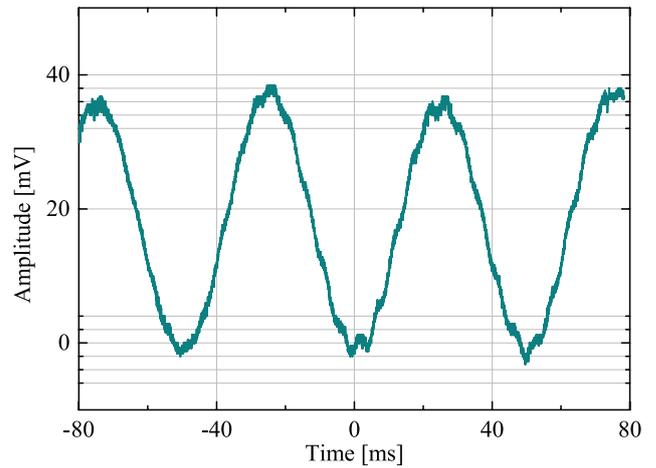
Figure 9. Cantilever tip response to a 10 Hz excitation voltage.

As expected, the resonance along the vertical direction is stronger than that along the lateral direction. It can be explained by the fact that: first, rectangular cross section results in a higher area moment of inertia along the lateral direction; and second, the net DEP force along the lateral direction caused by position variation of cantilever off the central line of the V groove is relatively small compared to the DEP force normal to the field lines.

The bandwidth of the primary resonance along the vertical direction is about 5 Hz, implying a weakly damped system. A comparison between modeling and experiment of resonances are shown in tables 1 and 2.

Within the possible measurement variations of the cantilever thickness affecting the modeled modes, there is a good agreement between the model and the experiment.

The time domain transient response is measured using impulse inputs and step inputs.

An impulse of 1 Hz is applied to study the damping of the cantilever. As shown in figure 11, the calculated exponential time constant is about 60 ms, hence the damping ratio is 0.013. The quality factor is evaluated to be about 40.

The step response is studied by applying a falling edge step input from 60 V to 0 V with comparison to the response by applying a rising edge step input from 0 V to 60 V.

We measure an averaged settling time of 2 ms and 200 ms for a rising edge input and a falling edge input, respectively (shown in figure 12). The rising edge response is much faster than the falling edge one.

One reason accounting for the faster rising edge response is the air damping [19]. As the cantilever oscillates, the nontrivial air film between the V shape groove and the cantilever is squeezed and sheared causing a built-up force against the motion of the cantilever. Considering the significantly long air film along the cantilever, this air damping may become significant when the cantilever is closer to the groove walls as in the case of a rising edge stimulus.

The most possible reason is the 'dynamic stiffness' change after a rising edge input. Considering a second order mass-damping-stiffness model for the dynamic system:

$$m\ddot{y} + d\dot{y} + k(y)y = 0 \quad (13)$$
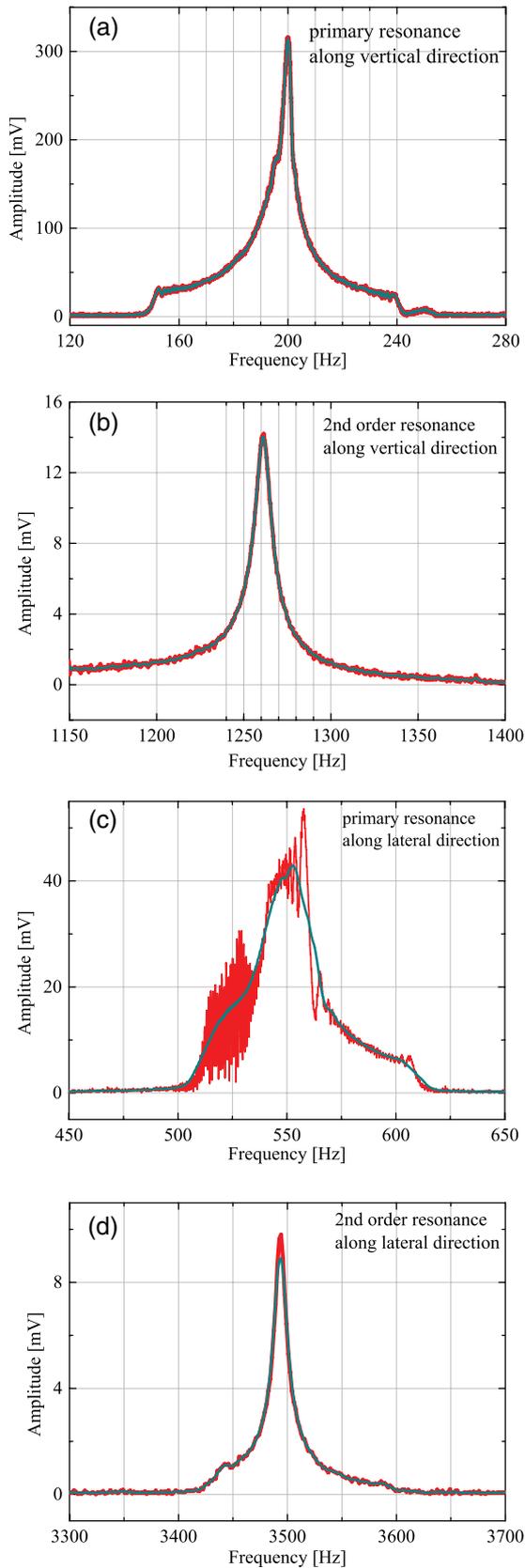
Figure 10. (a) and (b): First two resonances of the cantilever along the vertical direction. (c) and (d): First two resonances of cantilever along the lateral direction.

Table 1. First four resonances along the vertical direction: modeling and measurement.

Vertical resonance frequency [Hz]	1st order	2nd order	3rd order	4th order
Modeling	202	1267	3549	6955
Experiment	200	1262	3525	6995

Table 2. First two resonances along the lateral direction: modeling and measurement.

Lateral resonance frequency [Hz]	1st order	2nd order
Modeling	563	3528
Experiment	552	3494
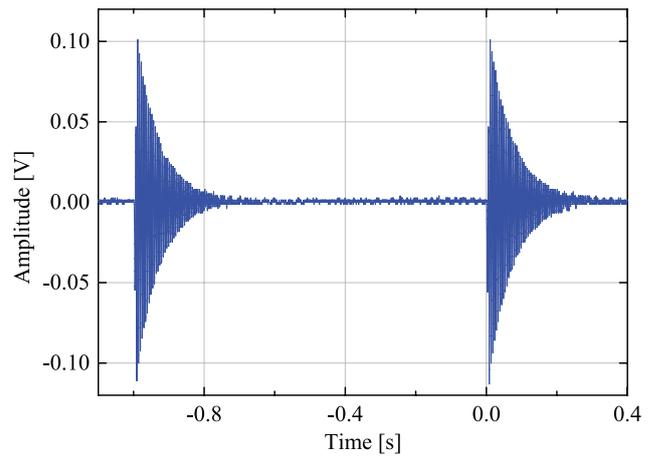
Figure 11. Impulse response at 1 Hz.

where m is the mass, d is the damping coefficient and $k(y)$ is the spring. When applying a rising input from 0 V to 60 V, the consequent driving force proportional to the cube of the reciprocal of the position increases quickly in its magnitude as the cantilever reacts to move down. This effect adds nonlinearity to the stiffness and reduces the effective stiffness dynamically. As a consequence, the system is gradually damped eventually closing to critical damping, resulting in much faster settling time.

Fused silica has a high mechanical strength and a high quality factor [20], so it will naturally oscillate for longer time as indicated from figure 12(a). However, the damping, caused by dynamically loading of the cantilever, leads to the cantilever to settle quicker. It suggests that input shaping method [19] can be adopted to tune the settling time and the positioning speed for a desirable response; it also indicates that the working configuration of the actuator under tension is favorable.

4. Conclusion

A monolithic 3D transparent micro-actuator is fabricated by femtosecond laser micromachining of fused silica and fully demonstrated.
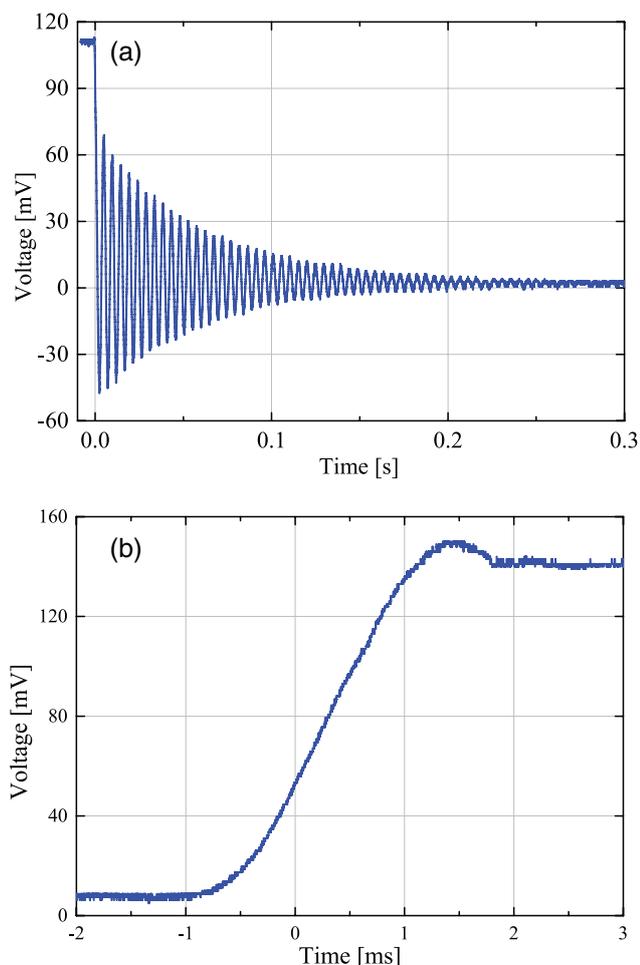
Figure 12. (a) Step response in seconds for a falling edge input. (b) The response in milli-seconds for a rising edge input.

DEP actuation inherits the advantages of electrostatic actuation: high compactness, high simplicity and low power consumption. It is also capable of 2D or even 3D motion by proper arrangement of stationary electrodes and at the same time suppresses the need for electrodes on non-conductive, mobile components, which make it superior to traditional electrostatic actuations.

The high mechanical strength and high transparency of fused silica over a broad wavelength, as an added value, offer transparent DEP actuators high integration and multi-function potentials, promising in but not limited to adaptive optics and integrated optics.

On the other hand, for voltage-driven scheme of DEP actuation, issues like low force output, limited traveling distance set by its inherent instability and scaling, may limit its implementation for various occasions but also inspire further efforts in improvements.

The DEP actuator reported here can be used for implementing various functions such as optical switching and coupling [21]. Using femtosecond laser machining, DEP actuation schemes can further be monolithically integrated in photonics circuits [22–24] or in devices combining waveguides and fluidics channels [25, 26] as well as devices combining waveguides and other functional elements such as

flexures [27], resonators [28] or other optical elements such as Fresnel lenses [29] and spherical lenses [30].

References

[1] Liu C 2005 *Foundations of MEMS* (Englewood Cliffs, NY: Prentice-Hall)
[2] Bellouard Y 2009 *Microrobotics: Methods and Applications* (Boca Raton, FL: CRC Press)
[3] Dudus A, Blue R, Zagnoni M, Stewart G and Uttamchandani D 2015 *IEEE J. Sel. Top. Quantum Electron.* **21** 4500209
[4] Candiani A, Konstantaki M, Margulis W and Pissadakis S 2012 *Opt. Lett.* **37** 4467–9
[5] Lenssen B and Bellouard Y 2012 *Appl. Phys. Lett.* **101** 103503
[6] Pohl H A 1951 *J. Appl. Phys.* **22** 869–71
[7] Pethig R 2010 *Biomicrofludics* **4** 022811
[8] Lian Z *et al* 2012 *Opt. Exp.* **20** 29386–94
[9] Burek M J, Ramos D, Patel P, Frank lan W and Loncar M 2013 *Appl. Phys. Lett.* **103** 131904
[10] Jebens R, Trimmer W and Walker J 1989 *Sensors Actuators* **20** 65–73
[11] Pohl H A 1958 *J. Appl. Phys.* **29** 1182–8
[12] Winter W T and Welland M E 2009 *J. Phys. D: Appl. Phys.* **42** 045501
[13] Morishima K, Fukuda T, Arai F, Ishihara H, Matsuura H and Yoshikawa K 1995 *Proc. 6th Int. Symp. on Micro Machine and Human Science* (Nagoya: IEEE) pp 145–52
[14] Lin W and Zhao Y 2007 *Sensors* **7** 3012–26
[15] Pethig R and Markx G H 1997 *Trends Biotechnol.* **15** 426–32
[16] Moser R, Wuthrich R, Sache L, Higuchi T and Bleuler H 2003 *J. Appl. Phys.* **93** 8945–51
[17] Poncharal P, Wang Z L, Ugarte D and de Heer W A 1999 *Science* **283** 1513–6
[18] Han S M, Benaroya H and Wei T 1999 *J. Sound Vib.* **225** 935–88
[19] Mol L, Rocha L A, Cretu E and Wolffenbuttel R F 2009 *J. Micromech. Microeng.* **19** 074020
[20] Bellouard Y 2011 *Opt. Mater. Exp.* **1** 816–31
[21] Kikuya Y, Hirano M, Koyabu K and Ohira F 1993 *Opt. Lett.* **18** 864–6
[22] Minoshima K, Kowalevicz A M, Hartl I, Ippen E P and Fujimoto J G 2001 *Opt. Lett.* **26** 1516–8
[23] Thomson R R, Kar A K and Allington-Smith J 2009 *Opt. Exp.* **17** 1963–9
[24] Marshall G D, Politi A, Matthews J C F, Dekker P, Ams M, Withford M J and O'Brien J L 2009 *Opt. Exp.* **17** 12546–54
[25] Bellouard Y, Said A, Dugan M and Bado P 2003 *Proc. of Materials Research Society Symp.* (*Warrendale, USA*) vol 782 pp 63–8
[26] Schaap A, Rohrlack T and Bellouard Y 2012 *Lab Chip* **12** 1527–32
[27] Bellouard Y, Said A and Bado P 2005 *Opt. Exp.* **13** 6635–44
[28] Tang J, Lin J, Song J, Fang Z, Wang M, Liao Y, Qiao L and Cheng Y 2015 *Int. J. Optomechatron.* **9** 187–94
[29] Bricchi E, Mills J D, Kazansky P G, Klappauf B G and Baumberg J J 2002 *Opt. Lett.* **27** 2200–2
[30] Drs J, Kishi T and Bellouard Y 2015 *Opt. Exp.* **23** 17355–66